Applied Catalysis B: Environmental 162 (2015) 66–74

Contents lists available at ScienceDirect

Applied Catalysis B: Environmental

journal homepage: www.elsevier.com/locate/apcatb

N-modified TiO_2 photocatalytic activity towards diphenhydramine degradation and *Escherichia coli* inactivation in aqueous solutions

Ricardo A.R. Monteiro[a], Sandra M. Miranda[a,b,c], Vítor J.P. Vilar[a,*], Luisa M. Pastrana-Martínez[b], Pedro B. Tavares[e], Rui A.R. Boaventura[a], Joaquim L. Faria[b], Eugénia Pinto[c,d], Adrián M.T. Silva[b,*]

[a] *LSRE – Laboratory of Separation and Reaction Engineering, Associate Laboratory LSRE/LCM, Faculdade de Engenharia, Universidade do Porto, Rua Dr. Roberto Frias, 4200-465 Porto, Portugal*
[b] *LCM – Laboratory of Catalysis and Materials, Associate Laboratory LSRE/LCM, Faculdade de Engenharia, Universidade do Porto, Rua Dr. Roberto Frias, 4200-465 Porto, Portugal*
[c] *CEQUIMED/Laboratory of Microbiology, Biological Sciences Department, Faculty of Pharmacy of University of Porto, Rua Jorge Viterbo Ferreira 228, 4050-313 Porto, Portugal*
[d] *Interdisciplinary Centre of Marine and Environmental Research (CIIMAR/CIMAR), University of Porto, Rua dos Bragas 289, 4050-123 Porto, Portugal*
[e] *CQVR Centro de Química – Vila Real, Departamento de Química, Universidade de Trás-os-Montes e Alto Douro, 5000-801 Vila Real, Portugal*

ARTICLE INFO

Article history:
Received 3 March 2014
Received in revised form 28 May 2014
Accepted 14 June 2014
Available online 20 June 2014

Keywords:
Photocatalysis
Nitrogen modified TiO_2
Diphenhydramine
Escherichia coli

ABSTRACT

Nitrogen modified TiO_2 samples were prepared by grinding the benchmark TiO_2 photocatalyst (P25, Evonik Degussa Corporation) with different amounts of urea and applying calcination temperatures between 340 and 420 °C. Several characterization techniques, including X-ray photoelectron spectroscopy (XPS), N_2 porosimetry, X-ray diffraction (XRD), scanning electronic microscopy (SEM), and diffuse reflectance UV–vis spectroscopy (UV-DRS), were used to obtain information about the morphology, crystalline phases of TiO_2 and chemical binding of nitrogen. Nitrogen modification did not affect the crystalline phase of TiO_2 as far as XRD analysis concerns; on the other hand the modified materials developed an absorption in the visible part of the electromagnetic spectrum. The material with a urea:TiO_2 weight ratio of 1:2, calcined at 380 °C, exhibited the highest photocatalytic activity under visible light illumination ($\lambda > 430$ nm), towards degradation of diphenhydramine, an emerging water pollutant of pharmaceutical origin. The measured band gap energy of the material was 2.99 eV, which is in-line with observed optical absorption properties. In addition, this photocatalyst was also the most efficient for complete inactivation of *Escherichia coli* in aqueous solution when ultraviolet radiation ($\lambda = 365$ nm) was used. From the XPS analysis on the chemical states of this photocatalyst it is concluded that nitrogen is interstitial to the TiO_2 structure.

1. Introduction

TiO_2 is a semiconductor with unique optoelectronic and physiochemical properties, which have been, since the early of the 20th century, alluring the industry in many different applications [1–3]. In 1956, Kato and Mashio [4] conducted several studies dealing with oxidation reactions induced by TiO_2 under illumination. Later, in the 1960s, the TiO_2 photochemical effect was also explored to induce electrochemical reactions [5,6]. Following the example of natural photosynthesis, Fujishima succeeded in 1969 to photoelectrochemically decompose water over TiO_2, a breakthrough finding published in a restricted Japanese journal [7]. Only in 1972, Fujishima and Honda described for the first time the photoelectrochemical decomposition of water under light radiation and without any applied electric current, using a single TiO_2-rutile crystal (*n*-type semiconductor) as photoanode and a Pt counter electrode [8]. The interest of photocatalytic processes on environmental applications escalated after Frank and Bard [9] in 1977 examined the possibilities of using TiO_2 to decompose cyanide in water. Thereafter, photocatalytic reactions have attracted increasing attention not only for many different water/wastewater treatment applications but also in the fields of energy conversion and air purification [10–17].

With a band gap of 3.2 eV, the photocatalytic activation of TiO_2 under solar irradiance is limited to the UV fraction of natural sunlight ($\lambda < 400$ nm), which represents roughly ~4% of the total

* Corresponding authors. Tel.: +351 220414908.
E-mail addresses: vilar@fe.up.pt (V.J.P. Vilar), adrian@fe.up.pt (A.M.T. Silva).

http://dx.doi.org/10.1016/j.apcatb.2014.06.017
0926-3373/

Sun irradiance reaching Earth's surface. In recent years, lot of attention has been paid towards shifting the absorption of TiO_2 based materials deeper into the visible region of the electromagnetic spectrum, where lies near 42% of the Sun's total irradiance. Several approaches have been described in the literature to achieve this goal, including doping or impregnation of metal ions into TiO_2 [18–21], reduction of TiO_2 via plasma treatments [22,23], combination of TiO_2 with other semiconductors or with carbon materials [24–27], and non-metallic doping of TiO_2 (C, F, N, S) [28–39].

Theoretical calculations for substitutional doping of C, N, F, P or S for O in the TiO_2 anatase phase, later confirmed by spectroscopic techniques [28], pointed out $TiO_{2-x}N_x$ (powders and films) as very promising photocatalysts for visible light activation (>500 nm). As early as 1986, Sato [37] reported the superior photoactivity of the nitrogen modified TiO_2 with relation to the benchmark P25 (TiO_2) material under visible light illumination. Since then, several methods for doping TiO_2 with nitrogen have been developed, such as ion implantation [38,40–42], sputtering [43–45], mechanical milling [46–48], chemical vapour deposition [49,50], sol–gel synthesis [37,51–55] and decomposition of nitrogen-containing metallorganic precursors [56–58].

Despite the general agreement found in the literature regarding the improvement of the TiO_2 photocatalytic activity driven by the incorporation of nitrogen, this enhancement has not been always observed. For example, the incorporation of β-substitutional nitrogen in N-doped TiO_2 was confirmed by XPS in the study of Yates et al. [59], however no relevant photocatalytic activity under visible light was observed. Frach et al. [60] also reported a lack of visible light activity for N-doped TiO_2. In fact, the photocatalytic activity of N-doped TiO_2 materials depends on several factors, with the preparation methods and precursors employed playing an unequivocally critical role on the resulting photocatalytic properties [57].

In this context, there is an on-going discussion on how nitrogen incorporation enhances the photocatalytic activity of TiO_2 under visible illumination [54,61–65]. Due to the different chemical nature of nitrogen doping species [52,53,66–69], it is important to understand the following concepts: (a) whether the incorporation is interstitial or substitutional; (b) if these species will diffuse to the surface of TiO_2; or (c) will be incorporated at the sub-surface or in bulk sites [55,70]. The location of the nitrogen species into the TiO_2 structure and their interaction with material matrix will strongly affect the material photocatalytic activity.

The electronic structure of the doped material has also been an issue in discussion. One point of view states that incorporation of nitrogen shifts the adsorption edge to lower energies narrowing its band gap [28,43,71]; other authors opposed that the absorption in the visible region is due to the electronic transitions, from localized impurity states in the band gap, to the conduction band [33,54,61,72]. Moreover, Livraghi et al. [70] found that N-doped TiO_2 contains a single atom nitrogen centre in the bulk of TiO_2, promoting absorption in the visible region and electron transfer from the band gap to the conduction band, as well as to electron scavengers adsorbed at the surface of TiO_2.

The majority of these studies has been performed with organic pollutants, whereas the anti-microbial properties of N-doped TiO_2 materials have received much less attention [30,73–75]. Liu et al. [73] compared N-doped TiO_2 materials prepared by the sol–gel method and P25 towards *Escherichia coli* inactivation under visible light illumination; the results showed higher efficiency of the N-doped TiO_2. Rizzo et al. [75] also showed the higher photocatalytic inactivation of an *E. coli* strain that is antibiotic resistant, when using N-doped TiO_2 in comparison to commercially available TiO_2 photocatalysts (Millennium PC50 and PC100). Cheng et al. [74] reported the inactivation of more than 99% of *E. coli* and *Staphylococcus aureus* over N-doped TiO_2. Rengifo-Herrera and Pulgarin [30] also reported a high photocatalytic activity of N,S co-doped and N-doped commercial anatase TiO_2 powders towards *E. coli* inactivation under visible light illumination; in this case, the efficiency of such materials was similar to that obtained with the benchmark P25.

In the present work, nitrogen modified TiO_2 powders were modified with different urea amounts and calcined at different temperatures, in order to optimize the method for the synthesis of an active photocatalyst. Scanning electron microscopy (SEM), diffuse reflectance UV–vis spectroscopy (UV-DRS), X-ray diffraction (XRD), X-ray photoelectron spectroscopy (XPS), surface area and porosity measurements, were performed on the as-prepared samples. For the first time, the photocatalytic activity of these nitrogen modified TiO_2 materials is systematically confirmed, under visible light illumination, in the degradation of diphenhydramine, an emerging water pollutant. The selected samples were also tested under ultraviolet radiation, towards the inactivation of *E. coli*.

2. Experimental

2.1. Chemicals

The high-purity (99%) analytical grade pharmaceutical selected for this study, diphenhydramine (DP) hydrochloride (2-diphenylmethoxy-*N*,*N*-dimethylethanamine hydrochloride), was supplied by Sigma–Aldrich. The properties of DP are already listed elsewhere [76]. Potassium hydroxide (>90%) and tert-butanol (≥99.7%) were obtained from Fluka, Sigma–Aldrich. Hydrochloric acid (37%) was purchased from Pronalab. EDTA (ethylenediaminetetraacetic acid, >99%) was supplied by Fisher Scientific. Acetonitrile (≥99.8%) was used with HPLC grade (Chromanorm). P25 (TiO_2, 80% anatase, 20% rutile) from Evonik Degussa Corporation, urea (reagent grade, 98%) from Sigma–Aldrich and ethanol (99.8%) from AGA were employed without further purification. Ultrapure water was produced in a Direct-Q Millipore® system.

2.2. Catalyst preparation and characterization

The nitrogen modification of P25 was accomplished by classical impregnation with urea. An amount of 1.0 g P25 was mixed with 0.10–3.0 g of urea and then 60 mL of ethanol were added under stirring until complete evaporation of the solvent. A calcination step of 2 h was also performed. Samples were labelled as N_xP25-*y* where *x* represents the weight of urea in grams (up to 3.0 g) and *y* represents the calcination temperature in °C (typically 380 °C). To investigate the effect of the calcination temperature, the sample prepared with 0.50 g of urea was also thermally treated at 340 °C and 420 °C. These samples were respectively denoted as $N_{0.50}$P25-340 and $N_{0.50}$P25-420.

The optical properties of the samples were analyzed by UV–vis diffuse reflectance spectroscopy (UV-DRS) using a JASCO V-560 UV/Vis spectrophotometer, equipped with an integrating sphere attachment (JASCO ISV-469). The reflectance spectra were converted by the instrument software (JASCO) to equivalent absorption Kubelka-Munk units. Barium sulphate was used as a reference.

The surface area measurements were performed in a Quantachrome NOVA 4200e porosimeter using N_2 at −196 °C. Before analysis, the samples were outgassed overnight at 150 °C. Surface areas were calculated from the N_2 adsorption isotherms using the Brunauer–Emmett–Teller (BET) method (S_{BET}). The micropore surface areas were calculated using the *t*-plot method and the pore size distribution was obtained using the Barrett–Joyner–Halenda (BJH) analysis from the desorption branch [77–79]; while this method is more appropriate for type IV isotherms, it was used in the present work to compare the samples.

The morphology of the samples was observed by scanning electron microscopy (SEM) coupled with energy dispersive X-ray (EDS) analysis, using a FEI Quanta 400 FEG ESEM/EDAX Genesis X4 M apparatus equipped with a Schottky field emission gun (for optimal spatial resolution). The samples were mounted on a carbon double-sided adhesive tape and observed at different magnifications.

X-ray diffraction (XRD) analysis was carried out in a PANalytical X'Pert MPD equipped with a X'Celerator detector and secondary monochromator (Cu Kα $\lambda = 0.154$ nm, 50 V, 40 A; data recorded at a 0.017 step size, 100 s/step). Rietveld refinement with Powder Cell software (CCP14, UK) was used to identify the crystallographic phases present and to calculate the crystallite size from the XRD diffraction patterns.

X-ray photoelectron spectroscopy (XPS) analysis was performed using a Kratos AXIS Ultra HSA, with VISION software for data acquisition and CASAXPS software for data analysis. The analysis was carried out with a monochromatic Al Kα X-ray source (1486.7 eV), operating at 15 kV (90 W), in FAT mode (Fixed Analyser Transmission), with a pass energy of 40 eV for regions ROI and 80 eV for survey. Data acquisition was performed with a pressure lower than 1×10^{-6} Pa, and it was used a charge neutralization system. The deconvolution of the spectra was performed using the XPSPEAK41 program, in which an adjustment of the peaks was considered using peak fitting with Gaussian-Lorentzian peak shape and Shirley type background subtraction.

2.3. Analytical technique

The concentration of DP was analyzed by HPLC with a Hitachi Elite LaChrom system equipped with a Hydrosphere C18 column (250 mm × 4.6 mm; 5 μm particles) maintained at room temperature, a Diode Array Detector (L-2450) and a solvent delivery pump (L-2130). An isocratic method set at a flow rate of 1 mL min^{-1} was used with the eluent consisting of an A:B (70:30) mixture of 20 mM NaH_2PO_4 acidified with H_3PO_4 at pH 2.80 (A) and acetonitrile (B). Absorbance was found to be linear over the whole range of measurement. The maximum relative standard deviation of HPLC measurements was never larger than 2%.

2.4. Photocatalytic experiments

2.4.1. Diphenhydramine photocatalytic degradation

The photocatalytic efficiencies of the samples were evaluated in the degradation of 10 mg L^{-1} DP (absorption at $\lambda < 280$ nm) at room temperature (25 °C) under visible light illumination. A Heraeus TQ 150 medium-pressure mercury vapour lamp ($\lambda_{exc} = 254$, 313, 366, 436 and 546 nm) was held in a quartz immersion tube located inside a DURAN® glass water-cooling jacket. A cut-off long pass filter ($\lambda > 430$ nm) was used to block the longer wavelengths. The photon flow entering the reactor was ca. 2.86 mW cm^{-2} as determined by integrating the irradiance spectrum using a UV–vis spectroradiometer (USB2000+, OceanOptics, USA).

The batch experiments were performed in a glass reactor filled with 7.5 mL of DP solution. The initial pH of the DP solution was 5.9 (variations lower than 0.4 were observed at the end of the experiments) and at these pH values (i.e. below 7.0) DP protonated form is the only specie present in solution [26]. The suspension was magnetically stirred and continuously purged with an oxygen flow to maintain oxygen saturation. The load of catalyst was kept at the optimal value of 1.0 g L^{-1} determined for degradation of DP with P25 [26].

Prior to irradiation, the suspension was magnetically stirred for 30 min under dark conditions to establish the adsorption–desorption equilibrium. After equilibration, the concentration of the substrate was measured and that value taken as the initial concentration ($C_{DP,0}$). The dark adsorption (discarded by this method) was never larger than 20% of the initial amount of pollutant loaded. Then, the lamp was turned on. Samples were taken from the reactor at different reaction times and centrifuged at 14,000 rpm for 10 min to separate the catalyst particles before being analyzed. A control experiment, in the absence of catalyst, was also performed as a blank run in order to account for direct photolysis. A pseudo-first order kinetic model often used in photocatalysis [80–82], was used as described by the following equation:

$$C_{DP,t} = C_{DP,0} e^{-kt} \quad (1)$$

where k is the apparent pseudo-first order kinetic constant, t is the reaction time and $C_{DP,0}$ and $C_{DP,t}$ denote the DP concentration at $t = 0$ and $t = t$, respectively.

The k constants obtained by fitting the model described in Eq. (1) to the normalized DP concentration histories ($C_{DP,t}/C_{DP,0}$) as well as the coefficient of variation, CV, expressed in percentage as k_{CV} (standard error × 100/parameter value) and the corresponding regression coefficient (r^2), are gathered in Table 1.

Table 1
Pseudo first-order kinetic constant (k), respective coefficient of variation (CV), expressed as a percentage (k_{CV}), and regression coefficient (r^2) of DP degradation under visible light illumination.

Catalyst	k [10^{-3} min^{-1}]	k_{CV} [%]	r^2
None	0.30 ± 0.05	6.1	0.97
$N_{0.10}$P25-380	3.2 ± 0.2	5.8	0.96
$N_{0.25}$P25-380	4.2 ± 0.3	6.8	0.95
$N_{0.40}$P25-380	5.6 ± 0.2	3.1	0.99
$N_{0.50}$P25-380	8.7 ± 0.5	5.3	0.97
$N_{0.60}$P25-380	7.1 ± 0.4	5.6	0.97
$N_{0.75}$P25-380	6.2 ± 0.5	7.9	0.94
$N_{1.0}$P25-380	6.2 ± 0.2	3.9	0.98
$N_{2.0}$P25-380	1.6 ± 0.1	4.5	0.98
$N_{3.0}$P25-380	0.7 ± 0.4	6.0	0.96
P25	0.51 ± 0.06	12	0.90
$N_{0.50}$P25-340	4.6 ± 0.1	2.0	0.99
$N_{0.50}$P25-420	2.7 ± 0.1	2.3	0.99

2.4.2. Bacterial inactivation tests

E. coli ATCC 25922 was used for the microbiological tests and the "spread plate method" was employed to evaluate the photocatalysts antibacterial activity. This method consisted of spreading 100 μL of a suspension of a given photocatalyst (0.125 mg mL^{-1} and 0.500 mg mL^{-1}) and *E. coli* cells into Mueller-Hinton agar (MH, Merck, Germany) plates. Before each experiment, *E. coli* was inoculated into MH agar and incubated overnight at 37 °C. A suspension of *E. coli* cells was prepared and diluted in saline solution to approximately 10^3–10^4 colony-forming units (CFU) mL^{-1}.

Inactivation tests were carried out in a 6 wells microtiter plate where 1 mL of the photocatalyst suspension was added to 1 mL of the *E. coli* cells suspension. The microtiter plate was placed at a distance of 3.60 cm from a UVA lamp (Sylvania Lynx-s 11 W black-light blue lamp with a spectral peak of 365 nm; photon flux of ca 25 W_{UV} m^{-2}). The UVA photon flux was measured in several points located at 3.6 cm of the UVA lamp, using a broadband UV radiometer (CUV 5, Kipp & Zonen B.V.); the radiometer was plugged to a hand-held display unit (Meteon, Kipp & Zonen B.V.) to produce readings in terms of UVA photon flux. All experiments were performed at room temperature and the suspensions magnetically stirred throughout the experimental period to ensure adequate mixing and contact between the photocatalyst and *E. coli* cells. Under UVA light radiation, samples for cell counting were collected at $t = 0$, 5, 10, 15 and 20 min. Samples without growth after photocatalytic treatment were re-suspended in MH broth for evaluation of the photocatalyst bactericidal effect: the cultures were incubated at 37 °C during 24 h and 100 μL were spread into MH agar plates to evaluate viable

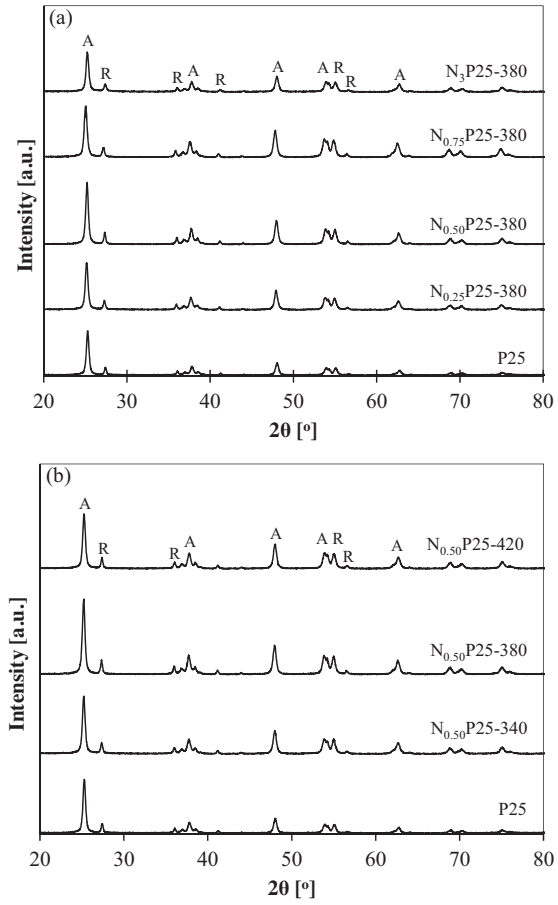

Fig. 1. XRD patterns of the samples synthesized with different (a) urea contents and (b) calcination temperatures. XRD pattern of P25 is also shown as reference. A: anatase; R: rutile.

bacteria. Control experiments in the dark and under UVA light in the absence of photocatalyst were also performed. All the results obtained were confirmed in triplicate.

3. Results and discussion

3.1. Characterization

The XRD patterns of the different N_xP25-*y* samples as well as of the bare P25 sample, used as reference, are shown in Fig. 1. In comparison with P25, no new diffraction peaks were observed in the samples prepared with different amounts of urea (Fig. 1a). Apparently, the modification with nitrogen does not affect the crystalline TiO_2 forms of P25 (anatase and rutile), which is in agreement with results previously described in the literature [33,83,84]. However, for the nitrogen-containing samples it is visible that the intensities of the peaks are slightly different from those of bare P25, suggesting some modification by the treatment performed. Fig. 1b shows that the crystalline forms of TiO_2 also remained similar when samples were subjected to different calcination temperatures (i.e. $N_{0.50}$P25-340, $N_{0.50}$P25-380 and $N_{0.50}$P25-420).

The phase composition and crystallite sizes of the different samples, estimated by the Williamson–Hall equation [85] are listed in Table 2. All nitrogen-containing samples present lower percentage of anatase crystalline phase and higher percentage of rutile crystalline phase when compared with P25. At the same time, the anatase and rutile crystallites are in general smaller than those of P25 (as observed previously when hydrothermal/solvothermal methods were used to prepare TiO_2 and nitrogen-modified TiO_2 samples [35,86]), except for the $N_{0.50}$P25-380 sample in which the rutile crystallite size is, by far, the highest (50 nm) among all the samples.

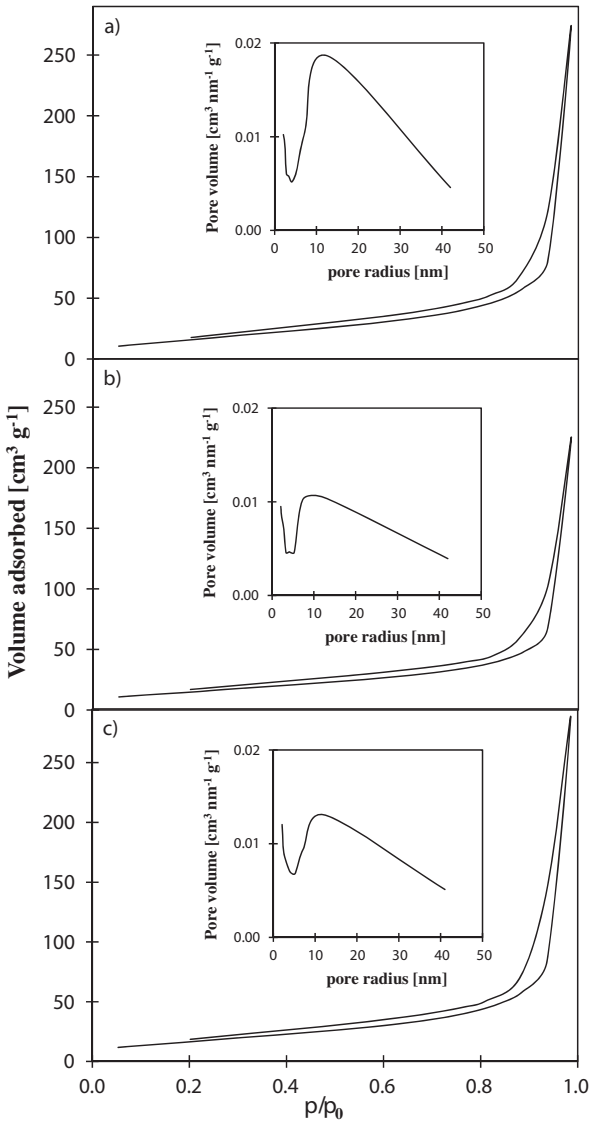

Fig. 2. N_2 adsorption–desorption isotherms and pore size distribution (inset) of: (a) $N_{0.75}$P25-380, (b) $N_{0.50}$P25-380 and (c) $N_{0.25}$P25-380.

Fig. 2 shows the nitrogen adsorption–desorption isotherms of N_xP25-380 samples. The pore size distributions were computed by the BJH analysis method from the desorption branch of the isotherm (Fig. 2 inset). All samples have similar specific surface areas (around 62 $m^2\ g^{-1}$, Table 2) and the isotherms are of type II [87], exhibiting a hysteresis loop at high relative pressures between 0.8 and 1.0 indicating the presence of mesopores. In the inset of Fig. 2, a clear pore size distribution with maximum pore radius between 10 and 15 nm is observed.

The spectra obtained through UV-DRS for bare P25 and N_xP25-380 samples prepared with different amounts of urea are depicted in Fig. 3a. The samples $N_{0.50}TiO_2$-380 and $N_{0.75}$P25-380 presented a significant absorption tail in the visible region between 400 and 600 nm, which is the typical absorption feature of N-doped TiO_2 materials. Thus, for these samples, the modification of TiO_2 with nitrogen resulted in a red shift of the absorbance region. According to some authors [1,2,61] this phenomenon is due to the substitution on the lattice of oxygen by nitrogen during the TiO_2 nitridation, narrowing the band gap by mixing the N2p and the O2p states.

Table 2
Optical, structural and textural properties of N_xP25-*y* and bare P25.

Sample	N_2 physisorption		XRD		UV–vis	
	S_{BET}[a] [$m^2\ g^{-1}$]	$r_{p,BJH}$[a] [nm]	Phase composition[b] [v/v %]	Crystallite size[b] [nm]	Absorption threshold [nm]	E_g [eV]
P25	61	15	86 (A), 14 (R)	32 (A), 44 (R)	382	3.25
$N_{0.25}$P25-380	63	12	82 (A), 18 (R)	28 (A), 37 (R)	397	3.13
$N_{0.50}$P25-380	61	10	85 (A), 15 (R)	30 (A), 50 (R)	415	2.99
$N_{0.75}$P25-380	63	13	82 (A), 18 (R)	26 (A), 30 (R)	403	3.08
$N_{0.50}$P25-340	–	–	81 (A), 19 (R)	32 (A), 32 (R)	412	3.02
$N_{0.50}$P25-420	–	–	84 (A), 16 (R)	29 (A), 45 (R)	405	3.07

[a] BET surface area (S_{BET}) calculated by Brunauer–Emmet–Teller (BET) formula and average pore diameter ($r_{p,BJH}$) calculated by Barrett–Joyner–Halenda (BJH) formula.
[b] A: anatase; R: rutile.

Another hypothesis, reported by Irie et al. [61] and by Sathish et al. [33], suggests the presence of an isolated narrow band above the valence band. In contrast, no significant absorption above 400 nm was observed for $N_{0.25}$P25-380, which may imply an ineffective modification of TiO_2 due to the low amount of urea used in this case.

The influence of the calcination temperature on the optical properties of $N_{0.50}$P25-y is shown in Fig. 3b. It can be observed that only the samples $N_{0.50}$P25-380 and $N_{0.50}$P25-340 present an absorption in the visible region, while no significant absorption was found for the sample calcined at the highest temperature (420 °C). The $N_{0.50}$P25-380 sample also presents the lowest band gap energy (2.99 eV in Table 2), making it potentially the most active photocatalyst. Fig. 4 shows SEM micrographs for this particular sample and the corresponding EDS spectrum. Agglomerates of spherical-like particles are observed on the micrographs while EDS analysis confirmed the presence of nitrogen on this sample. In addition, the particles size seems to be lower than 50 nm, in agreement with the XRD data and pore size distributions presented above. XPS analysis was also performed for this sample, and the results are shown in Fig. 5, together with those obtained for bare P25. N1s peaks in the range of 396–404 eV are considered typical of N–TiO_2 materials [5,6,33,47,54,56,88,89]. A N1s peak at 396–397 eV is often considered characteristic of Ti—N—Ti—N or Ti—N—Ti—O linkages, thus attributed to nitrogen replacing oxygen in the crystal lattice of TiO_2 [33,47,54,88,89]. A N1s peak at higher binding energy (398–400 eV) [33,88] is generally assigned to the presence of Ti—O—N and/or Ti—N—O bonds [33,54,88] where the electronic status of nitrogen is anion-like (N^-). Fig. 5a shows the deconvoluted N1s spectrum, where two peaks (at 399.0 and 400.3 eV) are observed. Considering the above mentioned discussion, these peaks may be attributed to Ti—O—N and/or Ti—N—O bonds, in this way suggesting nitrogen substitution into TiO_2 [33,86,90]. Regarding Ti2p and O1s core levels, respectively Fig. 5b and c, no differences were observed when comparing the $N_{0.50}$P25-380 sample and bare P25.

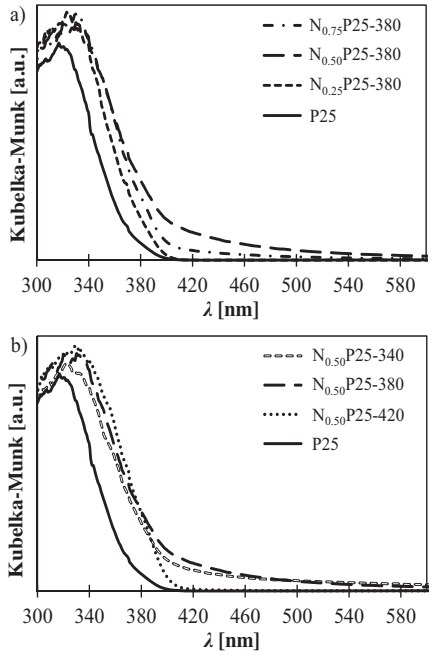

Fig. 3. UV–vis absorption spectra of: (a) $N_{0.25}$P25-380, $N_{0.50}$P25-380, $N_{0.75}$P25-380 and bare P25 and (b) $N_{0.50}$P25-340, $N_{0.50}$P25-380, $N_{0.50}$P25-420 and bare P25.

3.2. Diphenhydramine photocatalytic degradation

The samples obtained with a wide range of urea:TiO_2 weight ratios (up to 3:1), and also those treated at three different temperatures, together with bare P25, were studied in the photodegradation of DP under visible light illumination, i.e. at $\lambda > 430$ nm (Fig. 6). The respective pseudo-first order rate constants are shown in Table 1. It is worthy of note that DP is a very resistant pollutant in the absence of a catalyst, since the DP conversion observed in such case is less than 3% in 60 min (Fig. 6a).

The activity of the catalysts prepared with different amounts of urea follows the sequence (Fig. 6a and b respectively for small and large amounts of urea, and Table 1): $N_{0.50}$P25-380 ($8.7 \times 10^{-3}\ min^{-1}$) > $N_{0.60}$P25-380 ($7.1 \times 10^{-3}\ min^{-1}$) > $N_{0.75}$P25-380 ($6.2 \times 10^{-3}\ min^{-1}$) ~ $N_{1.0}$P25-380 ($6.2 \times 10^{-3}\ min^{-1}$) > $N_{0.40}$P25-380 ($5.6 \times 10^{-3}\ min^{-1}$) > $N_{0.25}$P25-380 ($4.2 \times 10^{-3}\ min^{-1}$) > $N_{0.10}$P25-380 ($3.2 \times 10^{-3}\ min^{-1}$) > $N_{2.0}$P25-380 ($1.6 \times 10^{-3}\ min^{-1}$) > $N_{3.0}$P25-380 ($0.7 \times 10^{-3}\ min^{-1}$) > P25 ($0.51 \times 10^{-3}\ min^{-1}$), where the values in brackets refer to the pseudo-first order rate constants. The results indicate the superior activity of all modified samples compared to P25 towards DP degradation under visible light illumination, and that the catalytic activity depends on the amount of urea employed in the preparation method, i.e. in the nitrogen content in TiO_2, considering that these materials were calcined at the same temperature. For instance, it is shown a clear increase in the pseudo-first order rate constant with the amount of urea ($N_{0.10}$P25-380 and $N_{0.50}$P25-380 samples), until a certain point where a clear decrease in pseudo-first order rate constants is then observed when the amount of urea is further increased ($N_{0.50}$P25-380 and $N_{3.0}$P25-380 samples). Thus, among the nitrogen modified samples, the highest pseudo-first order rate constant was obtained when 0.50 g of urea was used ($8.7 \times 10^{-3}\ min^{-1}$). The high photocatalytic activity of $N_{0.50}$P25-380 towards degradation of DP can be justified by the highest

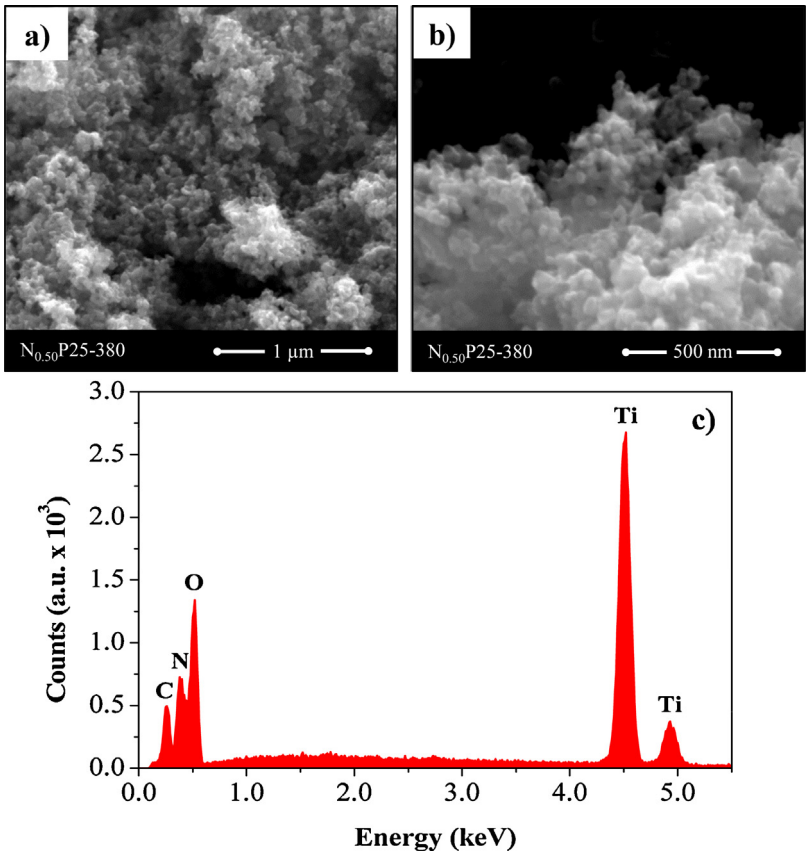

Fig. 4. (a and b) SEM micrographs at different magnifications, and (c) EDS spectrum of $N_{0.50}$P25-380.

red-shift of the absorption to the visible range observed in Fig. 3, corresponding to the lowest band gap energy (Table 2), originated by the substitution on the lattice of oxygen by nitrogen during the TiO_2 nitridation. In fact, the efficiency of these materials ($N_{0.50}$P25-380 > $N_{0.75}$P25-380 > $N_{0.25}$P25-380 > P25) followed the opposite trend with respect to the band gap energies indicated in brackets: $N_{0.50}$P25-380 (2.99 eV) < $N_{0.75}$P25-380 (3.08 eV) < $N_{0.25}$P25-380 (3.13 eV) < P25 (3.25 eV).

It is widely accepted that the treatment temperature used to prepare N-doped TiO_2 catalysts influences the photocatalytic activity [33,91]. Fig. 6c shows the effect of the thermal treatment on DP photocatalytic degradation with the samples prepared with a fixed amount of urea (0.50 g) and different calcination temperatures, i.e. 340, 380, and 420 °C. The photocatalytic activity was influenced by the calcination temperature, wherein the pseudo-first order rate constant increases from 340 °C to 380 °C but decreases from 380 °C to 420 °C (i.e. $k = 4.6 \times 10^{-3}$, 8.7×10^{-3} and 2.7×10^{-3} min^{-1} for $N_{0.50}$P25-340, $N_{0.50}$P25-380 and $N_{0.50}$P25-420, respectively, Table 1). Among these three samples, the lowest photocatalytic activity was found for $N_{0.50}$P25-420, being related with a lower amount of nitrogen in the TiO_2 structure due to the highest calcination temperature [92]. In fact, the sample calcined at 420 °C is less yellowish than those calcined at 340 °C and 380 °C, which may implies nitrogen depletion from the photocatalyst [91,92]. In contrast, the calcination at 340 °C may be not enough to decompose the nitrogen-precursor and incorporate nitrogen in the structure of TiO_2. Once again, the efficiency of the materials ($N_{0.50}$P25-380 > $N_{0.50}$P25-340 > $N_{0.50}$P25-420 > P25) followed the opposite trend of the band gap energies shown in brackets: $N_{0.50}$P25-380 (2.99 eV) < $N_{0.50}$P25-340 (3.02 eV) < $N_{0.50}$P25-420 (3.07 eV) < P25 (3.25 eV).

3.3. *E. coli* inactivation

Fig. 7 summarizes the photocatalytic effect of bare P25, $N_{0.25}$P25-380, $N_{0.50}$P25-380 and $N_{0.75}$P25-380 on the growth inhibition of *E. coli* under UVA. Two different photocatalyst loads were tested in order to assess their influence on the *E. coli* growth inhibition. All the photocatalysts tested showed very good antimicrobial activity against *E. coli* bacteria at the highest photocatalyst load tested (0.500 mg mL^{-1}), reducing more than 95% of CFU in 5 min and 100% in 10 min.

Reducing the photocatalyst load to 0.125 mg mL^{-1}, becomes evident that $N_{0.50}$P25-380 presents the highest inactivation efficiency towards *E. coli*, whereas P25 showed the lowest. Interestingly, these results for *E. coli* inactivation under UVA correlate well to those obtained for DP degradation under visible light illumination, where $N_{0.50}$P25-380 stands out as a better photocatalyst for the experimental conditions employed. The tested photocatalysts showed no effect under dark conditions as no *E. coli* inactivation was observed after 20 min without UVA light; the effect of the UVA lamp was also assessed and negligible *E. coli* inactivation was observed in the experiments performed under UVA light radiation without photocatalyst (data not shown). Furthermore, no bacteria growth was observed in the re-suspended samples incubated at 37 °C during 24 h. These results show the bactericidal effect of the photocatalyst on *E. coli*.

Rengifo-Herrera et al. [93] monitored the formation of hydroxyl ($HO^{\bullet}$) and superoxide (O_2^{-}) radicals by using electron spin resonance (ESR) studies with bare TiO_2 and N, S co-doped TiO_2 samples. The authors concluded that $HO^{\bullet}$ radicals were the main species involved in *E. coli* inactivation under UV (330–400). It was also suggested that the O_2^{-} radical and its oxidation product ($^1O_2$) were

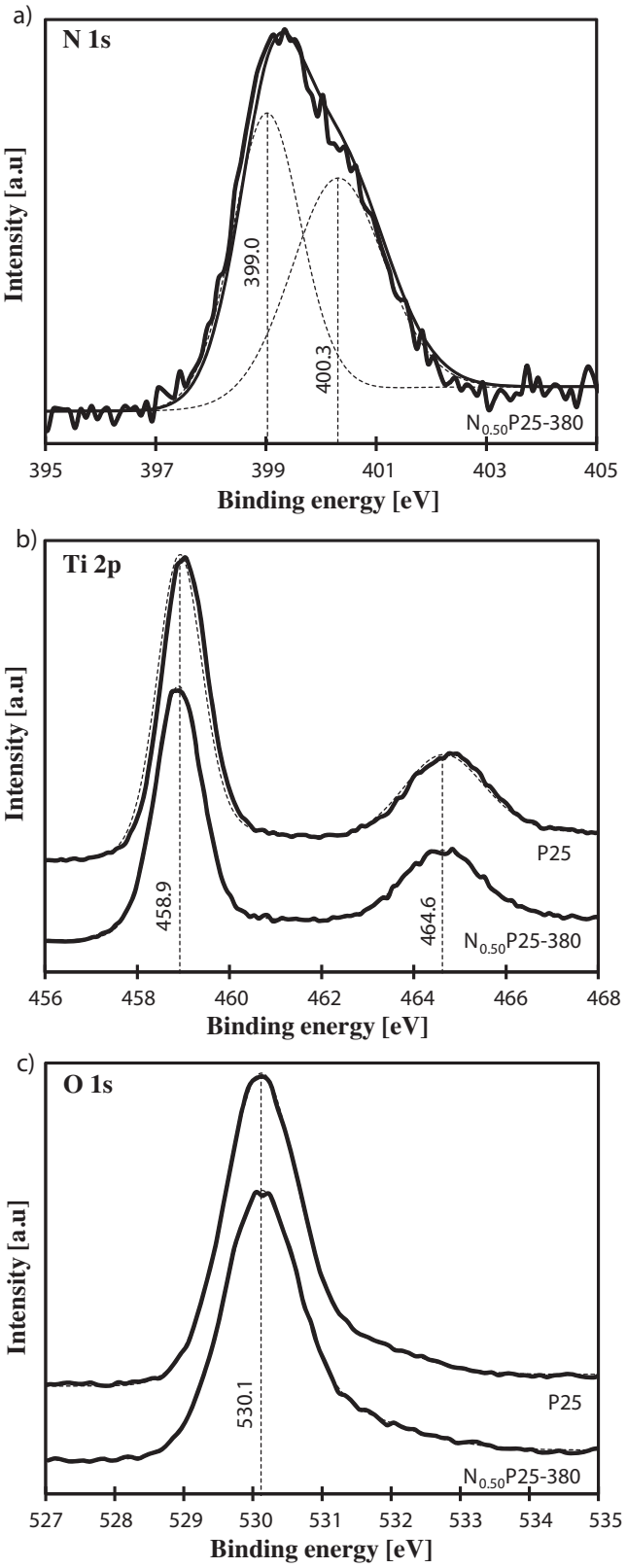

Fig. 5. X-ray photoelectron spectra of $N_{0.50}$P25-380 and bare P25 samples: (a) N1s, (b) Ti2p and (c) O1s core levels.

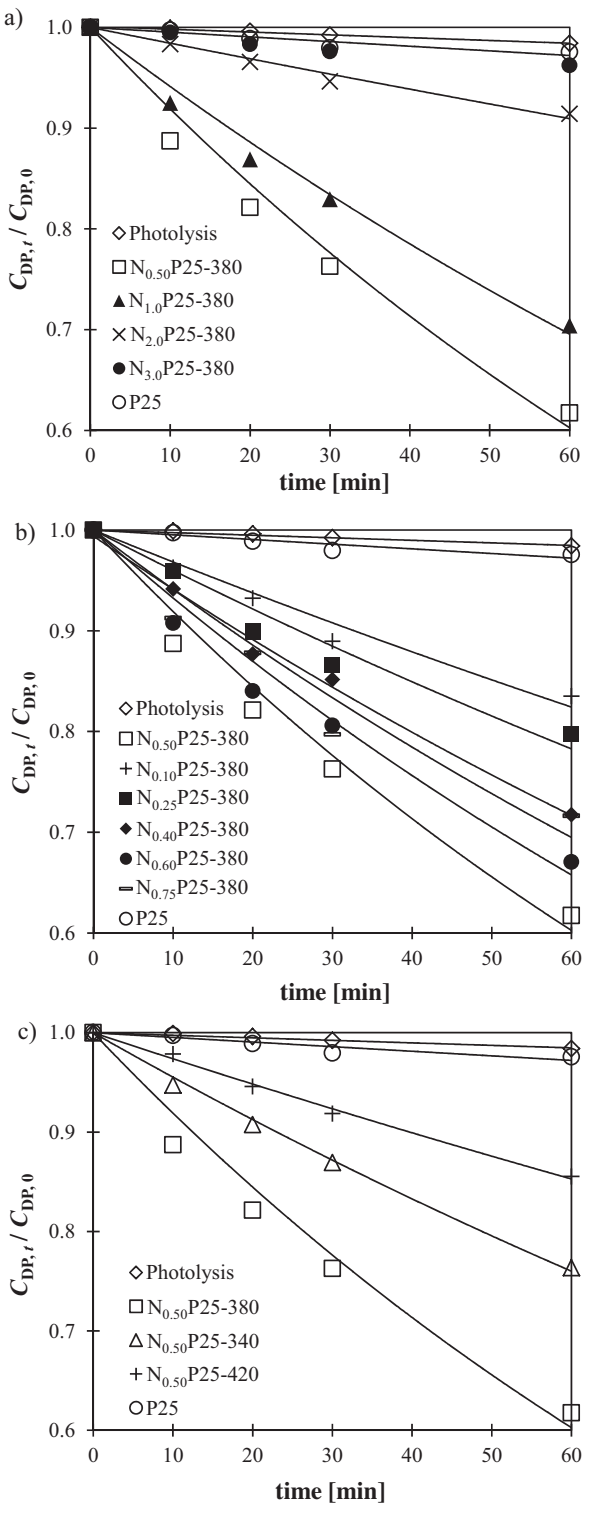

Fig. 6. Photocatalytic degradation of DP (10 mg L^{-1}) under visible light illumination for (a) and (b) materials prepared with different urea contents and (c) different temperatures (340, 380 and 420 °C). Catalyst load = 1.0 g L^{-1}. Curves represent the fitting of the pseudo-first order equation to the experimental data.

responsible for a marked *E. coli* inactivation with N, S co-doped TiO_2 under visible (400–500 nm) illumination. These conclusions are in agreement with other publications of the same authors dealing with (N-, S- and N-/S-) doped TiO_2 samples [30,94,95]. Therefore, the mechanisms involved under UV and visible light can be different; however, *E. coli* inactivation was observed in both cases regardless the main species involved. Since reactive species are produced with the $N_{0.50}$P25-380 sample under visible illumination (as shown by the significant DP degradation

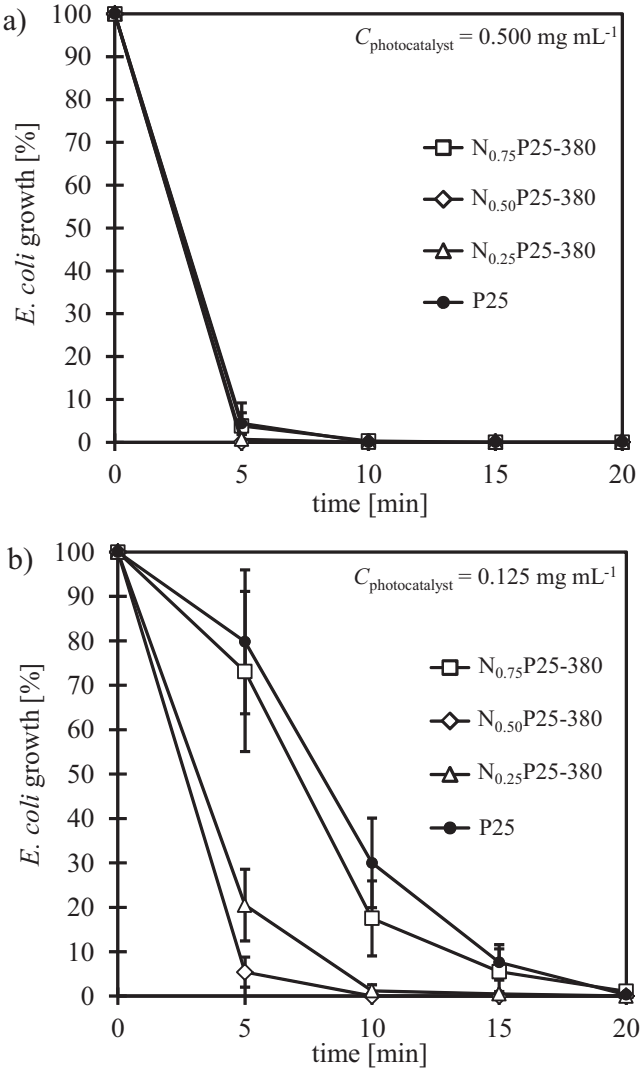

Fig. 7. *E. coli* growth under UVA for photocatalyst loads of (a) 0.500 mg mL^{-1} and (b) 0.125 mg mL^{-1}. Results are mean values (n = 3) and the error bars represent the standard deviation.

obtained in Fig. 6), *E. coli* inactivation under such conditions is also expected.

4. Conclusion

Effective visible light active nitrogen modified P25 photocatalysts were synthesized by a simple and low-cost preparation method, well suited for scale-up mass production.

From XPS analyses, it is shown that anion-like nitrogen (N^-) is present in the structure of TiO_2, as O—Ti—N and Ti—O—N linkages.

The catalytic activity for the degradation of a pharmaceutical pollutant, DP, under visible light illumination, and to inactivate *E. coli* bacteria, under UVA radiation, was found to depend on the amount of urea and calcination temperature used in the preparation method.

The material prepared with a urea:TiO_2 weight ratio of 1:2, and calcined at 380 °C, exhibits the highest photocatalytic efficiency for DP degradation and completely inactivates *E. coli* bacteria in 10 min. Further tests are needed in order to clarify the overall photocatalytic mechanism of nitrogen modified TiO_2 samples towards the elimination of harmful organic molecules and microorganisms inactivation.

Acknowledgements

Financial support for this work was mainly provided by the FCT (Fundação para a Ciência e a Tecnologia) project PTDC/EQU-EQU/100554/2008. This work was also supported by projects PEst-C/EQB/LA0020/2013, CEQUIMED-PEst-OE/SAU/UI4040/2014 and PEst-OE/QUI/UI0616/2014, financed by FCT and FEDER through COMPETE, and by QREN, ON2 (North Portugal Regional Operational Programme) and FEDER through projects NORTE-07-0162-FEDER-000050 and NORTE-07-0162-FEDER-000015. V.J.P. Vilar and A.M.T. Silva acknowledge the FCT Investigator 2013 Programme (IF/01501/2013 and IF/00273/2013, respectively), with financing from the European Social Fund and the Human Potential Operational Programme. R.A.R. Monteiro and L.M. Pastrana-Martínez gratefully acknowledge FCT for their PhD and Postdoctoral Research Fellowships, SFRH/BD/69323/2010 and SFRH/BPD/88964/2012, respectively. Technical assistance by Dr. Carlos Sá and CEMUP team with SEM and XPS/EDX analysis is gratefully acknowledged.

References

[1] E. Keidel, Furben Zeitung 34 (1929) 1242.
[2] C.F. Goodeve, J.A. Kitchener, Trans. Faraday Soc. 34 (1938) 570–579.
[3] A. Fujishima, K. Hashimoto, T. Watanabe, TiO_2 Photocatalysis: Fundamentals and Applications, Bkc Incorporated, Tokyo, 1999.
[4] S. Kato, F. Mashio, Abtr. Book Annu. Meet. Chem. Soc. Jpn. (1956) 223.
[5] H. Gerischer, in: H. Eyring, D. Henderson, W. Jost (Eds.), Physical Chemistry: An Advanced Treatise, Academic Press, New York, 1970, pp. 463–542.
[6] V.A. Myamlin, Y.V. Pleskov, Electrochemistry of Semiconductors, Plenum Press, New York, 1967.
[7] A. Fujishima, K. Honda, S. Kikuchi, J. Chem. Soc. Jpn. (Kogyo Kagaku Zasshi) 72 (1969) 108–113.
[8] A. Fujishima, K. Honda, Nature 238 (1972) 37–38.
[9] S.N. Frank, A.J. Bard, J. Am. Chem. Soc. 99 (1977) 303–304.
[10] C. Srinivasan, N. Somasundaram, Curr. Sci. 85 (2003) 1431–1438.
[11] D.Y. Goswami, J. Sol. Energy Eng. 119 (1997) 101–107.
[12] M.R. Hoffmann, S.T. Martin, W. Choi, D.W. Bahnemann, Chem. Rev. 95 (1995) 69–96.
[13] D.S. Bhatkhande, V.G. Pangarkar, A.A.C.M. Beenackers, J. Chem. Technol. Biotechnol. 77 (2002) 102–116.
[14] C. McCullagh, J. Robertson, D. Bahnemann, P. Robertson, Res. Chem. Intermed. 33 (2007) 359–375.
[15] D. Bahnemann, Sol. Energy 77 (2004) 445–459.
[16] R.W. Matthews, J. Chem. Soc. Faraday Trans. 80 (1) (1984) 457–471.
[17] J.-M. Herrmann, Top. Catal. 34 (2005) 49–65.
[18] A.K. Ghosh, H.P. Maruska, J. Electrochem. Soc. 124 (1977) 1516–1522.
[19] E. Borgarello, J. Kiwi, M. Graetzel, E. Pelizzetti, M. Visca, J. Am. Chem. Soc. 104 (1982) 2996–3002.
[20] M. Anpo, Pure Appl. Chem. 72 (2000) 1787–1792.
[21] H. Yamashita, M. Harada, J. Misaka, M. Takeuchi, Y. Ichihashi, F. Goto, M. Ishida, T. Sasaki, M. Anpo, J. Synchrotron Radiat. 8 (2001) 569–571.
[22] K. Takeuchi, I. Nakamura, O. Matsumoto, S. Sugihara, M. Ando, T. Ihara, Chem. Lett. 29 (2000) 1354–1355.
[23] T. Ihara, M. Miyoshi, M. Ando, S. Sugihara, Y. Iriyama, J. Mater. Sci. 36 (2001) 4201–4207.
[24] T. Hirai, K. Suzuki, I. Komasawa, J. Colloid Interface Sci. 244 (2001) 262–265.
[25] D. Chatterjee, A. Mahata, Appl. Catal. B: Environ. 33 (2001) 119–125.
[26] L.M. Pastrana-Martínez, S. Morales-Torres, V. Likodimos, J.L. Figueiredo, J.L. Faria, P. Falaras, A.M.T. Silva, Appl. Catal. B: Environ. 123–124 (2012) 241–256.
[27] L.M. Pastrana-Martínez, S. Morales-Torres, S.K. Papageorgiou, F.K. Katsaros, G.E. Romanos, J.L. Figueiredo, J.L. Faria, P. Falaras, A.M.T. Silva, Appl. Catal. B: Environ. 142–143 (2013) 101–111.
[28] R. Asahi, T. Morikawa, T. Ohwaki, K. Aoki, Y. Taga, Science 293 (2001) 269–271.
[29] T. Ohno, T. Mitsui, M. Matsumura, Chem. Lett. 32 (2003) 364–365.
[30] J.A. Rengifo-Herrera, C. Pulgarin, Sol. Energy 84 (2010) 37–43.
[31] Q. Xiao, L. Ouyang, J. Phys. Chem. Solids 72 (2011) 39–44.
[32] C. Burda, Y. Lou, X. Chen, A.C.S. Samia, J. Stout, J.L. Gole, Nano Lett. 3 (2003) 1049–1051.
[33] M. Sathish, B. Viswanathan, R.P. Viswanath, C.S. Gopinath, Chem. Mater. 17 (2005) 6349–6353.
[34] M. Mrowetz, W. Balcerski, A.J. Colussi, M.R. Hoffmann, J. Phys. Chem. B 108 (2004) 17269–17273.
[35] G. Yang, Z. Jiang, H. Shi, T. Xiao, Z. Yan, J. Mater. Chem. 20 (2010) 5301–5309.
[36] T. Cottineau, N. Bealu, P.-A. Gross, S.N. Pronkin, N. Keller, E.R. Savinova, V. Keller, J. Mater. Chem. A 1 (2013) 2151–2160.
[37] S. Sato, Chem. Phys. Lett. 123 (1986) 126–128.
[38] O. Diwald, T.L. Thompson, T. Zubkov, S.D. Walck, J.T. Yates, J. Phys. Chem. B 108 (2004) 6004–6008.

[39] V. Likodimos, C. Han, M. Pelaez, A.G. Kontos, G. Liu, D. Zhu, S. Liao, A.A. de la Cruz, K. O'Shea, P.S.M. Dunlop, J.A. Byrne, D.D. Dionysiou, P. Falaras, Ind. Eng. Chem. Res. 52 (2013) 13957–13964.
[40] M. Batzill, E.H. Morales, U. Diebold, Phys. Rev. Lett. 96 (2006) 026103.
[41] A. Ghicov, J.M. Macak, H. Tsuchiya, J. Kunze, V. Haeublein, L. Frey, P. Schmuki, Nano Lett. 6 (2006) 1080–1082.
[42] K. Yang, Y. Dai, B. Huang, J. Phys. Chem. 111 (2007) 12086–12090.
[43] Y. Nakano, T. Morikawa, T. Ohwaki, Y. Taga, Appl. Phys. Lett. 86 (2005) 132104.
[44] S.-Z. Chen, P.-Y. Zhang, D.-M. Zhuang, W.-P. Zhu, Catal. Commun. 5 (2004) 677–680.
[45] J. Premkumar, Chem. Mater. 16 (2004) 3980–3981.
[46] I.-C. Kang, Q. Zhang, S. Yin, T. Sato, F. Saito, Appl. Catal. B: Environ. 84 (2008) 570–576.
[47] S. Yin, K. Ihara, M. Komatsu, Q. Zhang, F. Saito, T. Kyotani, T. Sato, Solid State Commun. 137 (2006) 132–137.
[48] B. Liu, S. Yin, R. Li, Y. Wang, T. Sato, J. Ceram. Soc. Jpn. 115 (2007) 692–696.
[49] O. Diwald, T.L. Thompson, E.G. Goralski, S.D. Walck, J.T. Yates, J. Phys. Chem. B 108 (2003) 52–57.
[50] T. Tachikawa, Y. Takai, S. Tojo, M. Fujitsuka, H. Irie, K. Hashimoto, T. Majima, J. Phys. Chem. B 110 (2006) 13158–13165.
[51] C. Di Valentin, G. Pacchioni, A. Selloni, S. Livraghi, E. Giamello, J. Phys. Chem. B 109 (2005) 11414–11419.
[52] T. Imao, T. Horiuchi, N. Noma, S. Ito, J. Sol-Gel Sci. Technol. 39 (2006) 119–122.
[53] N. Venkatachalam, A. Vinu, S. Anandan, B. Arabindoo, V. Murugesan, J. Nanosci. Nanotechnol. 6 (2006) 2499–2507.
[54] S. Sakthivel, M. Janczarek, H. Kisch, J. Phys. Chem. B 108 (2004) 19384–19387.
[55] C. Di Valentin, E. Finazzi, G. Pacchioni, A. Selloni, S. Livraghi, M.C. Paganini, E. Giamello, Chem. Phys. 339 (2007) 44–56.
[56] C. Belver, R. Bellod, A. Fuerte, M. Fernández-García, Appl. Catal. B: Environ. 65 (2006) 301–308.
[57] D. Li, H. Haneda, S. Hishita, N. Ohashi, Mater. Sci. Eng. B 117 (2005) 67–75.
[58] T. Sano, N. Negishi, K. Koike, K. Takeuchi, S. Matsuzawa, J. Mater. Chem. 14 (2004) 380–384.
[59] H.M. Yates, M.G. Nolan, D.W. Sheel, M.E. Pemble, J. Photochem. Photobiol. A 179 (2006) 213–223.
[60] P. Frach, D. Glöß, M. Vergöhl, F. Neumann, K. Hund-Rinke, Proceeding of the 4th International Workshop on the Utilization and Commercialisation of Photocatalytic Systems (EJIPAC'04), 2004.
[61] H. Irie, Y. Watanabe, K. Hashimoto, J. Phys. Chem. B 107 (2003) 5483–5486.
[62] R. Nakamura, T. Tanaka, Y. Nakato, J. Phys. Chem. B 108 (2004) 10617–10620.
[63] C. Di Valentin, G. Pacchioni, A. Selloni, Phys. Rev. B 70 (2004) 085116.
[64] N. Serpone, J. Phys. Chem. B 110 (2006) 24287–24293.
[65] A.V. Emeline, N.V. Sheremetyeva, N.V. Khomchenko, V.K. Ryabchuk, N. Serpone, J. Phys. Chem. 111 (2007) 11456–11462.
[66] R. Bacsa, J. Kiwi, T. Ohno, P. Albers, V. Nadtochenko, J. Phys. Chem. B 109 (2005) 5994–6003.
[67] J.-h. Xu, W.-L. Dai, J. Li, Y. Cao, H. Li, H. He, K. Fan, Catal. Commun. 9 (2008) 146–152.
[68] H. Li, J. Li, Y. Huo, J. Phys. Chem. B 110 (2006) 1559–1565.
[69] K. Yamada, H. Nakamura, S. Matsushima, H. Yamane, T. Haishi, K. Ohira, K. Kumada, C. R. Chim. 9 (2006) 788–793.
[70] S. Livraghi, M.C. Paganini, E. Giamello, A. Selloni, C. Di Valentin, G. Pacchioni, J. Am. Chem. Soc. 128 (2006) 15666–15671.
[71] T. Morikawa, R. Asahi, T. Ohwaki, K. Aoki, Y. Taga, Jpn. J. Appl. Phys. 40 (2001) L561–L563.
[72] S. Sato, R. Nakamura, S. Abe, Appl. Catal. A: Gen. 284 (2005) 131–137.
[73] Y. Liu, J. Li, X. Qiu, C. Burda, Water Sci. Technol. 54 (2006) 47–54.
[74] X.L. Cheng, Y.J. Hu, S.J. Hu, L. Yu, G.R. Xie, Adv. Mater. Res. 189 (2011) 1258–1262.
[75] L. Rizzo, D. Sannino, V. Vaiano, O. Sacco, A. Scarpa, D. Pietrogiacomi, Appl. Catal. B: Environ. 144 (2014) 369–378.
[76] J.P. Berninger, B. Du, K.A. Connors, S.A. Eytcheson, M.A. Kolkmeier, K.N. Prosser, T.W. Valenti, C.K. Chambliss, B.W. Brooks, Environ. Toxicol. Chem. 30 (2011) 2065–2072.
[77] S. Brunauer, P.H. Emmett, E. Teller, J. Am. Chem. Soc. 60 (1938) 309–319.
[78] E.P. Barrett, L.G. Joyner, P.P. Halenda, J. Am. Chem. Soc. 73 (1951) 373–380.
[79] R.S. Mikhail, S. Brunauer, E.E. Bodor, J. Colloid Interface Sci. 26 (1968) 45–53.
[80] P. Zhang, J. Liu, J. Photochem. Photobiol. A 167 (2004) 87–94.
[81] B. Ohtani, J. Photochem. Photobiol. C 11 (2010) 157–178.
[82] J.-M. Herrmann, Environ. Sci. Pollut. Res. 19 (2012) 3655–3665.
[83] Y.V. Pleskov, Solar Energy Conversion: A Photochemical Approach, Springer Verlag, Berlin, 1990.
[84] J. Yuan, M. Chen, J. Shi, W. Shangguan, Int. J. Hydrogen Energy 31 (2006) 1326–1331.
[85] H. Bi, S. Li, Y. Zhang, Y. Du, J. Magn. Magn. Mater. 277 (2004) 363–367.
[86] F. Peng, L. Cai, L. Huang, H. Yu, H. Wang, J. Phys. Chem. Solids 69 (2008) 1657–1664.
[87] K.S.W. Sing, D.H. Everett, R.A.W. Haul, L. Moscou, R.A. Pierotti, J. Rouqueról, T. Siemieniewska, Pure Appl. Chem. 57 (1985) 603–619.
[88] X. Chen, C. Burda, J. Phys. Chem. B 108 (2004) 15446–15449.
[89] Y. Cong, J. Zhang, F. Chen, M. Anpo, J. Phys. Chem. 111 (2007) 6976–6982.
[90] H.U. Lee, S.C. Lee, S. Choi, B. Son, S.M. Lee, H.J. Kim, J. Lee, Chem. Eng. J. 228 (2013) 756–764.
[91] S. Yin, Y. Aita, M. Komatsu, T. Sato, J. Eur. Ceram. Soc. 26 (2006) 2735–2742.
[92] D. Wu, M. Long, W. Cai, C. Chen, Y. Wu, J. Alloys Compd. 502 (2010) 289–294.
[93] J.A. Rengifo-Herrera, K. Pierzchała, A. Sienkiewicz, L. Forró, J. Kiwi, C. Pulgarin, Appl. Catal. B: Environ. 88 (2009) 398–406.
[94] J.A. Rengifo-Herrera, J. Kiwi, C. Pulgarin, J. Photochem. Photobiol. A 205 (2009) 109–115.
[95] J.A. Rengifo-Herrera, E. Mielczarski, J. Mielczarski, N.C. Castillo, J. Kiwi, C. Pulgarin, Appl. Catal. B: Environ. 84 (2008) 448–456.